

Measurement of Near-Field Radiative Heat Transfer at Deep Sub-Wavelength Distances using Nanomechanical Resonators

Mathieu Giroux, Michel Stephan, Maxime Brazeau, Sean Molesky, Alejandro W. Rodriguez, Jacob J. Krich, Karin Hinzer, and Raphael St-Gelais*



Cite This: *Nano Lett.* 2023, 23, 8490–8497



Read Online

ACCESS |



Metrics & More

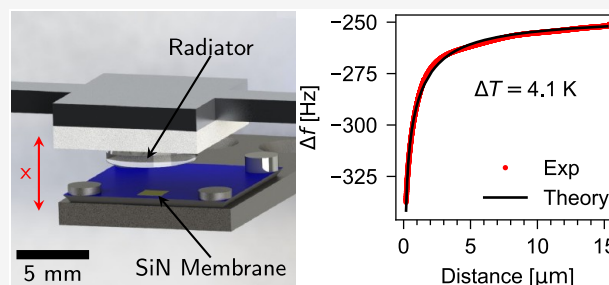


Article Recommendations



Supporting Information

ABSTRACT: Near-field radiative heat transfer (NFRHT) measurements often rely on custom microdevices that can be difficult to reproduce after their original demonstration. Here we study NFRHT using plain silicon nitride (SiN) membrane nanomechanical resonators—a widely available substrate used in applications such as electron microscopy and optomechanics—and on which other materials can easily be deposited. We report measurements down to a minimal distance of 180 nm between a large radius of curvature (15.5 mm) glass radiator and a SiN membrane resonator. At such deep sub-wavelength distance, heat transfer is dominated by surface polariton resonances over a (0.25 mm)² effective area, which is comparable to plane–plane experiments employing custom microfabricated devices. We also discuss how measurements using nanomechanical resonators create opportunities for simultaneously measuring near-field radiative heat transfer and thermal radiation forces (e.g., thermal corrections to Casimir forces).



KEYWORDS: Near-field radiation, nanomechanical resonators, thermal radiation, surface polariton

Near-field radiative heat transfer (NFRHT) has demonstrated great theoretical potential^{1–7} for applications such as energy conversion^{8–12} and heat transfer control.^{5–7,13} NFRHT consists of evanescent radiative thermal coupling occurring between two bodies at sub-wavelength distances. This evanescent coupling enables radiative heat transfer exceeding conventional laws of thermal radiation by orders of magnitude^{14–16} while being concentrated over a narrow spectral bandwidth.^{17–20}

Despite this large amount of promising theoretical work, technical challenges of precision alignment at high temperatures often limit experimental progress on NFRHT. Several approaches have been reported to mitigate or overcome experimental difficulties. While some used nanotips^{13,20–24} or microspheres^{25–31} to eliminate the need to maintain parallelism between the coupled surfaces, others relied on more customized designs to study NFRHT between parallel surfaces using active parallelism control^{32–40} or a custom nanofabricated static device.^{41–47} The development of static devices is key for achieving practical application of NFRHT. However, their custom-fabricated nature makes it difficult to integrate various new materials^{4,48–53} to experimentally study and confirm existing theoretical work on NFRHT. Since the majority of reported NFRHT experiments also employ custom nanodevices,^{13,23–26,32–35,41–47} experimental capabilities for investigating new materials for NFRHT remains limited. There is consequently a substantial imbalance between a large body

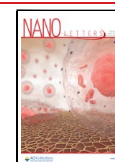
of theoretically investigated phenomena and relatively modest experimental capabilities in the field of NFRHT research.

In an effort to address this imbalance, we previously proposed an alternative⁵⁴ where the sensing element—a silicon nitride (SiN) membrane nanomechanical resonator—is a commonly available^{55,56} substrate material onto which other materials are routinely deposited, for example, in transmission electron microscopy. The high mechanical quality factor of these resonators and their high temperature sensitivity notably enabled the demonstration of a temperature resolution (1.2×10^{-6} K) unprecedented in the context of NFRHT measurements.⁵⁴ However, we did not achieve NFRHT in the deep sub-wavelength regime—where the thermal radiative heat transfer is dominated by surface polariton (SP) resonances—due to limited flexibility of our preliminary alignment platform (i.e., one-axis alignment, 25 nm step size, open-loop control). Other than potentially allowing material characterization, resonator-based sensing could offer a unique opportunity for measuring thermal radiation forces occurring in the context of near-field radiative heat transfer.^{57,58} SiN resonators already

Received: May 31, 2023

Revised: August 28, 2023

Published: September 6, 2023



allow, within the framework of optomechanics, strong coupling between radiation forces and mechanical excitation.⁵⁹ Likewise, SiN-based devices have been used to measure Casimir forces before⁶⁰ but not its out-of-equilibrium thermal contribution.⁵⁸

In this work, we present SiN membrane resonators as a platform for measuring NFRHT in the deep sub-wavelength regime and quantify their performance limits using a custom-built 5-axis positioning system (see Figure 1a). Our positioning

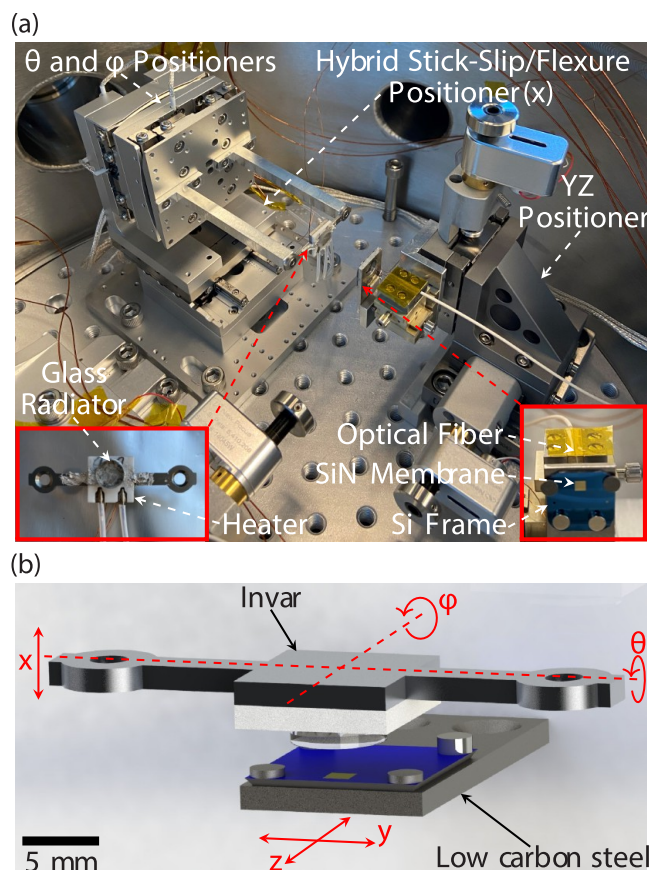


Figure 1. (a) NFRHT measurement apparatus inside the vacuum chamber. (b) Render of the NFRHT measurement platform showing both surfaces and the axes of motion used for the positioning. The glass radiator is mounted onto a metal ceramic heater, which is itself mounted on an Invar plate that minimizes required heating power and mechanical deformation. Silver paste is used as a conductive adhesive, which also helps dissipate any spurious electrostatic charges in the glass radiator. The SiN membrane resonator is mounted on a low carbon steel plate using 4 magnets, providing thermal grounding while limiting mechanical damping.

system enables the alignment of two surfaces in the y , z , θ , and ϕ direction, as shown in Figure 1b. The separation (x) between the two surfaces is controlled by a closed-loop hybrid linear stage (Smaract DLS-5252) that combines the advantages of long travel range (30 mm) stick–slip positioners and high-resolution piezoscanners, enabling a resolution of 1 nm over a 35 μm slip-free range. The y and z positions of the membrane can be modified using open-loop inertia drives (New Focus Picomotor) with 25 nm per step resolution. The θ and ϕ alignment of our platform is controlled by closed-loop stick–slip stages (Smaract SGO-60.5 and SGO-77.5), with 2 μ° resolution.

Other than the 5-axis positioning system, our platform relies on relatively simple components that are commercially available. The hot surface of our system is a BK7 glass lens (see Figure 1a) attached to a metal ceramic heater. The large radius of curvature of the glass radiator (15.5 mm), relative to previous probe-tip experiments,^{13,20–31} allows a large effective near-field heat transfer area (defined later in discussion related to Figure 4c) that is comparable to our membrane size and to previous microscale plate–plate experiments.^{10,34,35,47,61–63} The metal ceramic heater and spherical radiator are mounted on a custom-machined Invar plate, which, due to its low thermal conductivity and low thermal expansion coefficient compared to other metals, minimizes required heating power and mechanical deformation. The use of a spherical radiator eliminates the need for the θ and ϕ alignment axes in the current experiment, although their use is possible in future plane–plane experiments.

To measure the near-field radiation signal, we rely on a low-stress SiN membrane (built-in stress ~ 60 MPa, inferred from the mechanical resonance eigenfrequencies) with nominal dimensions of 1.7 mm in side length and $t_{\text{SiN}} = 100$ nm thickness. The SiN membrane used in this platform was fabricated in-house,⁶⁴ but comparable devices are available commercially.^{55,56} The temperature of the membrane is inferred in real time through an optical interferometer^{54,65} that measures shifts of the membrane mechanical resonance frequency due to thermally induced stress relaxation (i.e., material expansion).^{66,67} The membrane resonance frequency is tracked by phase locking (PLL) the internal oscillator of a lock-in amplifier (Zurich Instrument MFLI) to the membrane eigenfrequency.⁶⁸ The lock-in oscillator signal (set to an amplitude of 80 mV) is sent to a piece of piezoelectric ceramic (Thorlabs shear piezoelectric chip, PN:PLSFBP3) that actuates the membrane at its resonance frequency by acoustic coupling through the membrane-chip mount. The silicon frame of the membrane is mounted on a low carbon steel support (see Figure 1b) using 4 magnets, enabling good thermal contact for maintaining the silicon frame at room temperature, while limiting the mechanical damping compared to adhesive mounting. To suppress fluidic damping and convective heat transfer, the system is placed in a custom-designed high-vacuum chamber operating at a typical pressure of 2×10^{-6} Torr.

We predict the NFRHT signal between the radiator and the membrane using a model—discussed in greater detail in Supporting Information Section S.1 and ref 54—that combines the heat diffusion equation inside the membrane (eq S13),⁶⁹ multilayer NFRHT calculations,^{70,71} and the mechanical effects of nonuniform stress in the resonator obtained by solving the motion equation (eq S15).⁷² Far-field radiative heat transfer between the back side of the membrane and the surrounding is computed using conventional radiative heat transfer for small objects with large surroundings.⁷³ Far-field radiative heat transfer between the front side of the membrane and the radiator is calculated using the conventional far-field thermal radiation formalism⁷³ including geometrical view factors. In the near-field, we account for the curvature of the glass radiator using the proximity approximation (also known as the Derjaguin approximation⁷⁴) shown in eq S1. The permittivity of the glass radiator is taken from ref 75, and that of SiN is taken from ref 76.

Using this model, we compute a relative frequency sensitivity ($\Delta f/f_0$) of the membrane to temperature (and

absorbed radiation) of -7400 ± 900 ppm/K (-710 ± 90 ppm/ μ W), under far-field radiation. With a fundamental eigenmode frequency of ~ 58.5 kHz for our current membrane, the absolute frequency sensitivity is -433 ± 53 Hz/K (-41 ± 5 Hz/ μ W). In the near-field, these numbers change slightly due to a different temperature spatial distribution in the membrane. For example, at 200 nm near-field distance, the sensitivity is evaluated at -449 ± 55 Hz/K (-45 ± 5.5 Hz/ μ W) for our radiator geometry. The uncertainties result from the uncertainties in the material constants of SiN ($\alpha = 2.2 \pm 0.1 \times 10^{-6}$ K $^{-1}$,^{77–79} $\nu = 0.27 \pm 0.03$,^{77,79,80} $E = 300 \pm 30$ GPa,^{77–81} and $\rho = 3100 \pm 100$ kg/m³^{77,79,81}), for which values are not reported with more than two significant figures. Here α is the coefficient of thermal expansion, ν is the Poisson ratio, E is the Young modulus, and ρ is the density.

In the current geometry, mechanical frequency shifts due to Casimir forces are predicted to be much smaller than those due to NFRHT. The Casimir force (F_{cas}) and spring constant ($k_{\text{cas}} = \partial F_{\text{cas}}/\partial x$) are computed in Supporting Information Section S.2 using the model in ref 58. At a typical separation achieved in this work (~ 200 nm), the estimated shift (Δf_{cas}) of resonance frequency (f_0) due to Casimir forces is $\frac{\Delta f_{\text{cas}}}{f_0} \approx \frac{k_{\text{cas}}}{8\pi^2 m_{\text{eff}} f_0^2} \approx 20$ ppm. In comparison, typical temperature-induced frequency shifts (see Figure 2c) are on the order of 1300 ppm. We therefore neglect Casimir forces in the current work. However, we note that shifts on the order of 20 ppm can typically be resolved by our SiN membrane sensors, which have demonstrated stability smaller than 0.01 ppm in ref 82. If we can distinguish the contributions to frequency shifts due to Casimir and to NFRHT, our approach could provide a unique opportunity for measuring the never-demonstrated corrections to Casimir forces out of thermal equilibrium.⁵⁸

During the experiment, the proportional, integral, and derivative (PID) parameters of our closed-loop x -axis positioning system (see Figure 1b) are set to an overdamped mechanical response, preventing overshoot and oscillations of the positioner. This slow overdamped response also enables sampling of multiple temperature readings during displacement between two set points. During a typical $\tau_{\text{positioner}} \sim 2$ s displacement between two set points, as shown in Figure 2a, the membrane temperature is sampled 3350 times, yielding a temperature sampling every ~ 0.1 nm, even though the distance between the set points is 100 nm. We consider that the membrane remains in quasi-steady-state during these displacements since its characteristic thermal response time ($\tau_{\text{th}} \approx 0.066$ s⁸³) is much smaller than the positioner response time ($\tau_{\text{positioner}} \sim 2$ s). For even finer approaches, we use the same procedure but in 10 nm steps instead of 100 nm. These finer steps are typically used at smaller separation ($\lesssim 3$ μ m) to prevent accidental contact.

Transverse alignment (i.e., in YZ) of the apex of the glass radiator with the center of the membrane is critical for maximizing the membrane response to near-field radiation. Misalignment was the main limiting factor in our original 1-axis positioner concept demonstration,⁵⁴ but it is now no longer an issue with our 5-axis alignment platform. As the apex of the glass radiator is misaligned from the membrane center position, it becomes increasingly coupled to the silicon frame, thus, greatly reducing the near-field signal measured by the membrane. We rely on this effect to align the glass radiator apex with the membrane center. While actively

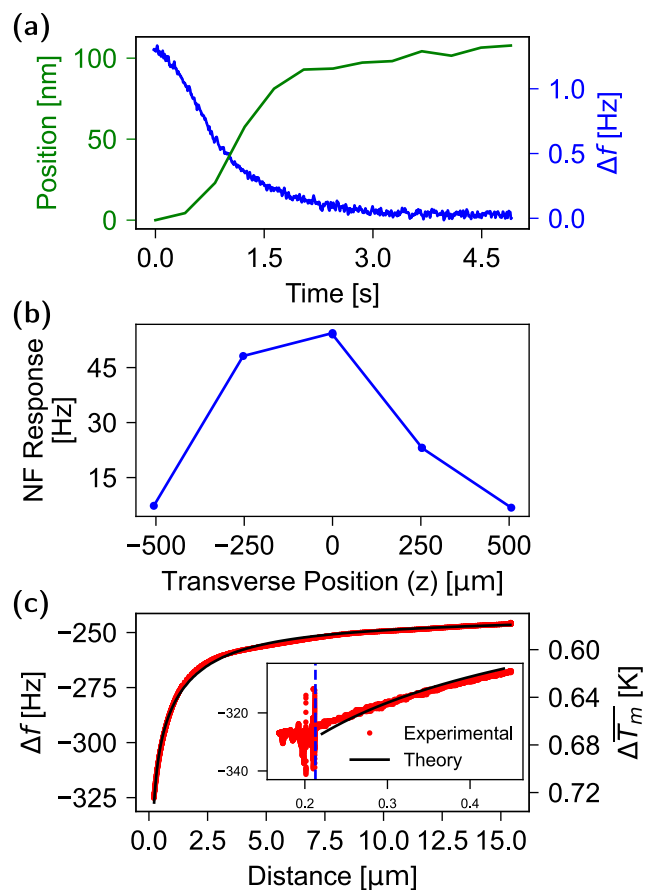


Figure 2. (a) Overdamped displacement response of the hybrid positioner as a function of time (in green). The frequency data (in blue) illustrates how we sample approximately 3350 points during a displacement between two set points separated by 100 nm. (b) Near-field (NF) response as a function of the transverse radiator position (z) demonstrating how we align the radiator apex with the membrane. The optimal position (where the near-field signal is maximized) is located at a z position of $0 \mu\text{m}$ with an uncertainty of $\pm 125 \mu\text{m}$. (c) Experimental (red) and theoretical (black) (fitted horizontally and vertically) resonance frequency shift as a function of separation for a $\Delta T = 4.0$ K temperature difference between the membrane and radiator. The fit suggests a minimal separation of ~ 210 nm. The initial shift of ~ 250 Hz at large distances results from the far-field radiative coupling. Inset: fluctuations at smaller distances lead to loss of mechanical resonance past the minimum gap of 210 nm. The dotted blue line identifies the position at which the resonance is lost.

recording the membrane frequency, we moved the glass radiator forward until the membrane mechanical resonance is lost. We then retracted the glass radiator by $15 \mu\text{m}$. Afterward, we use our Y (and Z) stage to adjust the horizontal (and vertical) positions of the hot surface by $250 \mu\text{m}$ and repeat the approach procedure while measuring the near-field signal. We repeat this procedure until the near-field radiation signal—i.e., the frequency shift before loss of resonance—is maximized (see Figure 2b). Once this procedure is completed, the apex of the glass radiator is aligned with the center of the membrane with an estimated accuracy of $\pm 125 \mu\text{m}$. With such uncertainty, our model⁵⁴ predicts negligible near-field signal degradation (less than 1% attenuation of the temperature signal compared to perfect alignment). We note that, due to the low temperature difference between the two surfaces ($\Delta T = 4.1$ K for the measurement in Figure 2b), measuring the

small shifts in temperature induced by 250 μm misalignments ($\Delta T_{\text{membrane}} \approx 0.014$ K) requires a high-resolution radiation sensor, like the SiN membrane (1.2×10^{-6} K⁵⁴) employed here.

Comparison of measured data with the model described above (Figure 2c, Figure 3) suggests that we reach a minimal

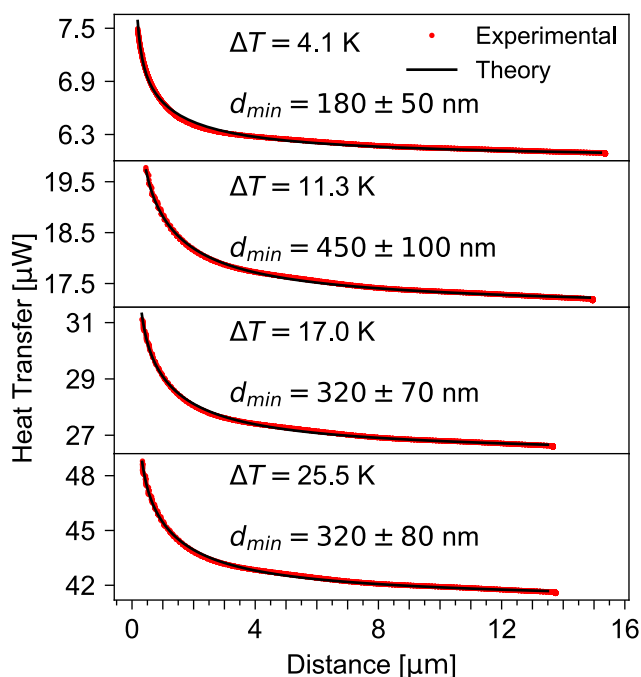


Figure 3. Experimental (red) and theoretical (black) (fitted horizontally and vertically) radiative heat transfer as a function of separation for different radiator-membrane temperature differences (ΔT) showing good correspondence with the theoretical model. The comparison with the theoretical model suggests that we have reached the deep sub-wavelength regime for all ΔT values. The minimal separation d_{min} achieved is identified in each plot.

distance $d_{\text{min}} = 180$ nm (see $\Delta T = 4.1$ K scan in Figure 3) between the membrane and the hot surface before we lose track of the membrane mechanical resonance (see typical loss of tracking in Figure 2c inset). The fit of the experimental data to the theoretical model accounts for three unknowns: (1) the radiator-membrane initial (far-field) distance, (2) the uncertainty of the far-field radiation intensity caused by the variety of materials present around the radiator (see Figure 1a inset), and (3) the temperature at the surface of the glass radiator. In Figure 2c, shifting the experimental data along the distance (horizontal) axis accounts for the first unknown. Likewise, shifting along the frequency shift (vertical) axis accounts for the second unknown while also correcting for slow frequency drift due to ambient temperature variation in the vacuum chamber. Finally, for the third unknown, fitting of the glass radiator surface temperature in the theoretical model results in an $\sim 50\%$ reduction compared to the temperature measured inside the metal ceramic heater. This reduction is most likely due to heat dissipation in the metal mount (see Figure 1b).

Our platform currently enables scans at temperature differences up to $\Delta T = 25.5$ K ($T_{\text{heater}} = 322.5$ K and $T_{\text{membrane}} = 297.0$ K), which is comparable to other macroscale NFRHT platforms reviewed in ref 61. For all scans with $\Delta T \leq 25.5$ K, the tip of the radiator reaches deep sub-wavelength distances

(see d_{min} values in Figure 3) where the thermal radiative heat transfer is dominated by SP resonances. Compared to previous membrane work, a smaller membrane (1.7 vs 3 mm in ref 54) was found to enable measurements at higher temperatures (25.5 vs 10 K in ref 54). The smaller membrane resulted in a better thermal ground from the silicon frame, allowing the membrane temperature to remain lower and less affected by far-field radiation. Still, the large size of our radiator is eventually limiting the maximum reachable temperature difference in our NFRHT measurement, as is also the case in other macroscale platforms.⁶¹ At temperature differences greater than 25.5 K, fluctuations and drift, induced by parasitic heating of the surroundings, eventually prevent continuous tracking of the membrane resonance frequency. This issue could possibly be mitigated by use of high-stress SiN resonators that are less temperature sensitive or by using smaller heaters/membranes that produce/capture less parasitic far-field radiation.

Due to the high resolution of our radiation sensor and positioning system, the accuracy of our minimum-distance results (d_{min} in Figure 3) is limited mainly by the uncertainty on material constants of SiN. During a sampling time typical of the displacement time between two set points (~ 2.5 s), the root-mean-square fluctuations of the x -axis position and frequency shift are, respectively, 3.6 nm and 0.026 Hz. These small fluctuations result in virtually noise-free curves (see Figure 2c and Figure 3) that can be fitted with our theoretical model to find the minimum distance achieved with a negligible influence from fluctuation noise. In contrast, the minimum distance extracted from this fit varies strongly with the uncertainties for the material constants of SiN (α , ν , E , ρ). These propagated uncertainties result in a 50 nm uncertainty of the minimal distance achieved, for a 4.1 K temperature difference. More information on uncertainty calculation is presented in Supporting Information: (Section S.3) position and frequency stability analysis, (Section S.4) separate optical measurement of the positioner response, and (Section S.5) propagation of uncertainty between SiN material constants and minimum distance achieved.

Reaching minimal distances in the 180–450 nm range (see Figure 3) implies that we transitioned into a regime where the radiative heat transfer is quasi-monochromatic, as is desirable in most NFRHT applications. As shown in Figure 4a,b the calculated spectral radiative heat flux, at 180 nm and $\Delta T = 4.1$ K, is dominated by a transverse magnetic polarization resonance at an angular frequency of $\omega = 9.24 \times 10^{13}$ rad/s. This resonance originates from surface polariton (SP) resonances in the glass radiator, since its parallel wavevector k_{p} exceeds both material light lines (given by $\text{Re}(n)k_0$,⁸⁴ where k_0 is the magnitude of the wavevector in vacuum and n is the refractive index of the material). In Figure 4c, we quantify the contribution of each of the components of the radiative heat flux at the tip of the radiator as a function of the separation. A similar analysis for the heat flux over the full area of the resonator is available in Supporting Information Section S.6. At a separation of 180 nm, the SP reaches a contribution of $91.4 \pm 4\%$ at the tip of the radiator, where the heat flux is therefore dominated by SP modes. We also show in Supporting Information Section S.7 that the 100 nm thickness of the membrane enhances the relative polariton contribution to heat transfer by a factor of 30% compared to bulk SiN, at a separation of 180 nm. Temperature-independent versions of the plots in Figure 4a,b are also reproduced in Supporting

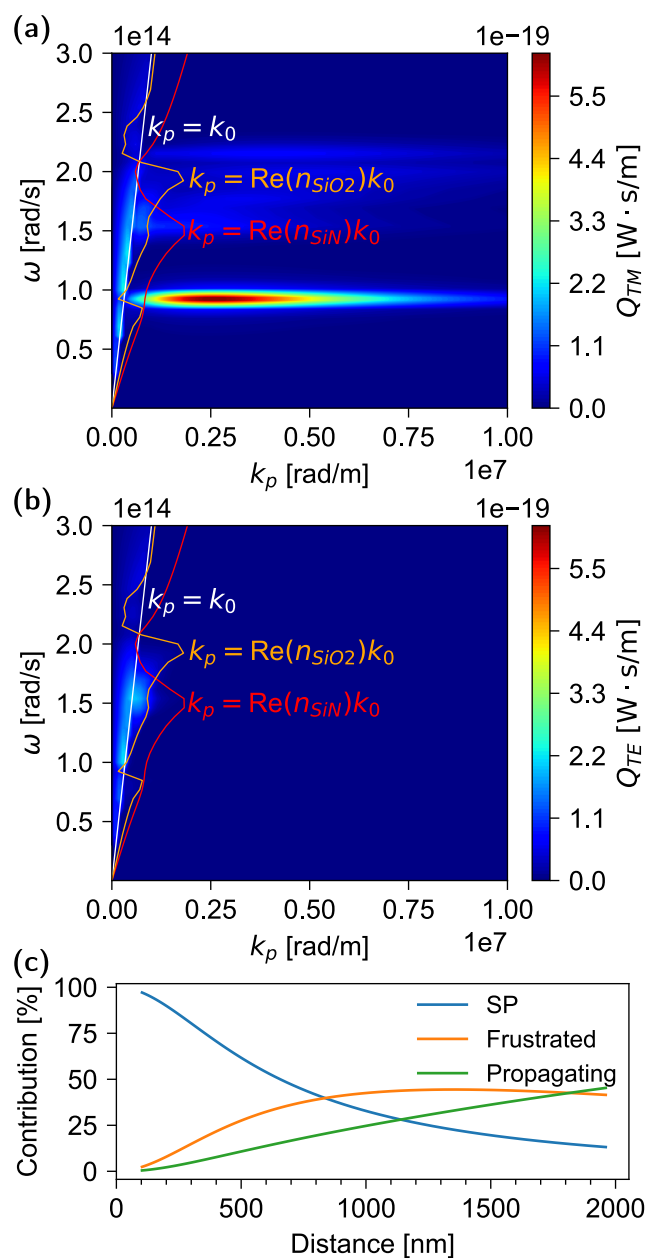


Figure 4. (a, b) Calculated radiative heat flux, at the radiator apex, per unit angular frequency, ω , and parallel wavevector, k_p , at 180 nm separation and a temperature difference of 4.1 K for (a) transverse magnetic (TM) and (b) transverse electric (TE) polarization. The propagating modes ($k_p < k_0$) and the frustrated modes ($k_0 < k_p < \min(\text{Re}(n_{\text{SiO}_2})k_0, \text{Re}(n_{\text{SiN}})k_0)$) have modest contributions (1.8% and 6.8%, respectively), while the SP mode ($k_p > \min(\text{Re}(n_{\text{SiO}_2})k_0, \text{Re}(n_{\text{SiN}})k_0)$) (accounting for 91.4% of the total radiative heat flux) is the dominating mode. (c) Contribution of each of the components of the radiative heat flux, at the tip of the radiator, as a function of distance for a 4.1 K temperature difference.

Information Section S.8 (i.e., the mode transmission only, not weighted by the Planck mean oscillator energy). Plots of the spectral heat flux for all gaps reported in Figure 3 can also be found in Supporting Information Section S.9.

Considering the minimal distances (d_{min}) achieved and the contribution of each radiative heat flux component (Figure 4), we infer a deep sub-wavelength effective area of $(0.25 \text{ mm})^2$ and a near-field heat transfer effective area of $(0.96 \text{ mm})^2$. We

define the former as the projected area of the radiator (at the apex) that is closer than 825 nm to the membrane (i.e., the distance in Figure 4 where the SP contribution becomes dominant). Interestingly, the resulting $(0.25 \text{ mm})^2$ is comparable to microscale plate–plate NFRHT experiments.^{10,34,35,47,61–63} Within this area, the total heat transfer is enhanced by a factor of 9 over the far-field intensity (see extended discussion in Supporting Information Section S.6). We also note that membranes with areas of $(0.25 \text{ mm})^2$ are a standard commercial product.⁵⁶ With such dimension, the entirety of the membrane area could be deep sub-wavelength-coupled to our radiator, as in a plate–plate experiment but without the need for θ , ϕ alignment. Predicted results for such membrane size are presented in Supporting Information Section S.6, showing that in this case SP contributions largely dominate over propagating mode contributions over the full area of the resonator. Conversely, we obtain the $(0.96 \text{ mm})^2$ area by calculating the projection of the radiator apex that is within a distance smaller than Wien’s wavelength ($\lambda_W = 9.7 \mu\text{m}$) from the membrane (i.e., the distance where near-field enhancement starts occurring due to frustrated waves). The resulting $(0.96 \text{ mm})^2$ is significantly larger than in all previous sphere-plane experiments,^{25–31} while also being comparable to our membrane size (1.7 mm side length).

Several factors could explain why we cannot measure near-field heat transfer at radiator-membrane distances below 180 nm. From Figure 2c, we note that, after mechanical resonance is intermittently lost, tracking of the frequency still averages over values that follow the general near-field trend. It is therefore possible that contact did not occur between the membrane and radiator, but that something else causes loss of frequency tracking. This hypothesis is strengthened by measurement of the surface flatness of the radiator and SiN (Figure 5), which show no asperities large enough for preventing near-field alignment beyond 180 nm. In Figure 5a, particles are detected on SiN, which are probably due to the fabrication process. Figure 5b shows the presence of longer engraved patterns on the surface of the radiator. Both are, however, much smaller than 180 nm.

Reasons, other than contact, that could cause a loss of frequency tracking are numerous and present interesting investigation directions. We first note that the resonator vibration amplitude (set to $\sim 2 \text{ nm}$ in the far-field by a 80 mV constant-amplitude modulation) sometimes drops (by up to 90%) as the system transitions from far-field to near-field coupling, making resonator frequency more difficult to track. This vibration dampening could originate either from parasitic effects (e.g., trapped charges on the membrane and/or radiator) or phenomena such as delayed thermal-Casimir forces⁵⁸ or bolometric backaction.⁸⁵ Additionally, in the deep sub-wavelength regime, spurious fluctuations of the membrane-radiator distance are strongly coupled to the membrane temperature (and hence to resonance frequency), potentially affecting PLL frequency tracking. Sources of such distance fluctuations include resonator actuation ($\sim 2 \text{ nm}$), fluctuation of the positioner (measured optically to $\sim 2.5 \text{ nm}$ over a 25 Hz bandwidth, see Supporting Information Section S.4), and thermomechanical fluctuation noise in the membrane ($\langle x \rangle = \sqrt{\frac{k_B T}{m_{\text{eff}} \omega_0^2}} = 0.012 \text{ nm}$). It is possible that smaller membrane dimensions (i.e., resulting in a stiffer membrane) could reduce several of these spurious effects (e.g., fewer trapped charges, fewer thermomechanical fluctuations, less deformation due to

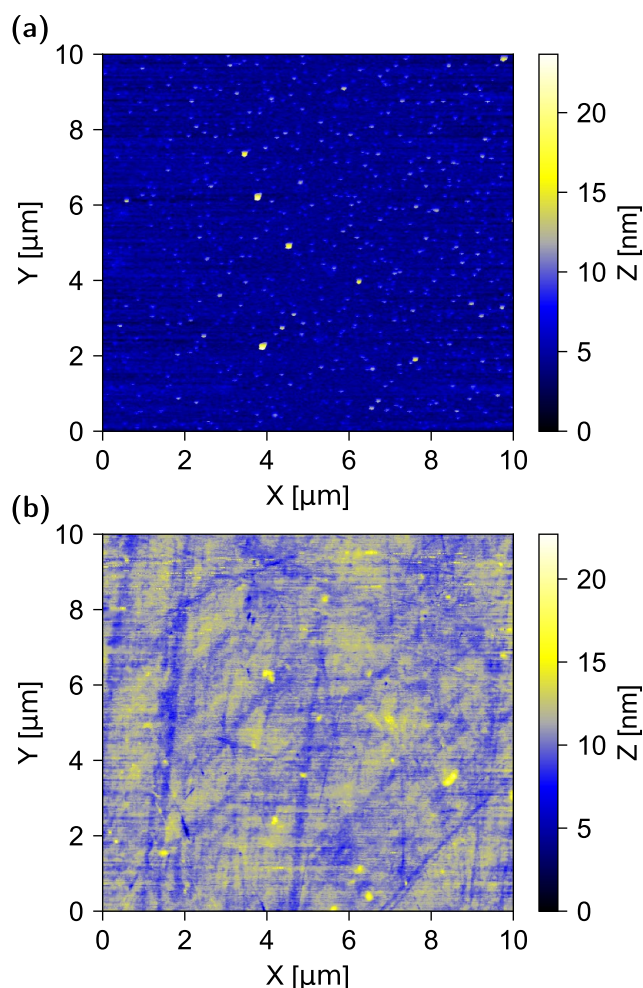


Figure 5. Atomic force microscopy measurements of (a) the SiN layer and (b) the radiator over a $100 \mu\text{m}^2$ surface area. Roughness on the order of ~ 24 and ~ 23 nm is observed in respective samples. SiN measurements are taken on SiN supported by the Si frame (i.e., not on the structurally released SiN) to prevent membrane destruction.

stiction forces). This remains to be confirmed experimentally but could allow measurement limited by the surface quality of our materials (i.e., at gaps < 50 nm according to Figure 5).

We have demonstrated that widely available SiN membrane resonators can enable near-field radiative heat transfer measurement in the deep sub-wavelength regime, over a $(0.25 \text{ mm})^2$ effective area, without custom nanofabricated devices. Such membrane size is widely available and can be used in future work to achieve deep sub-wavelength NFRHT measurement without the need for custom fabricated micro-devices. We therefore expect that the reproducibility and flexibility of our platform will facilitate investigation of new materials for NFRHT—such as graphene,⁴⁸ thin-film metals,⁴⁹ multilayers,⁵⁰ lossy materials,⁴ hyperbolic materials,^{51,52} and metamaterials⁵³—which can all be easily deposited on SiN membranes. The fact that nanomechanical resonators are sensitive to both force and temperature also creates an opportunity to investigate thermal corrections to the Casimir effect.

■ ASSOCIATED CONTENT

Supporting Information

The Supporting Information is available free of charge at <https://pubs.acs.org/doi/10.1021/acs.nanolett.3c02049>.

Theoretical model for mechanical frequency shifts due to NFRHT; Casimir forces estimation; stability analysis of positioner and SiN frequency; optical verification of the positioner displacement; uncertainty analysis; relative contributions of propagating, frustrated, and surface modes to total heat transfer; hybridization of surface polariton resonances in thin film SiN; Radiative heat transfer transmission coefficients; spectral distribution of radiative heat transfer (PDF)

■ AUTHOR INFORMATION

Corresponding Author

Raphael St-Gelais — Department of Mechanical Engineering, University of Ottawa, Ottawa, Ontario K1N 6N5, Canada; Department of Physics, University of Ottawa, Ottawa, Ontario K1N 6N5, Canada; orcid.org/0000-0003-0866-287X; Email: raphael.stgelais@uottawa.ca

Authors

Mathieu Giroux — Department of Mechanical Engineering, University of Ottawa, Ottawa, Ontario K1N 6N5, Canada; orcid.org/0000-0002-6792-9848

Michel Stephan — Department of Mechanical Engineering, University of Ottawa, Ottawa, Ontario K1N 6N5, Canada

Maxime Brazeau — Department of Mechanical Engineering, University of Ottawa, Ottawa, Ontario K1N 6N5, Canada

Sean Molesky — Department of Engineering Physics, Polytechnique Montreal, Montreal, Quebec H3T 1J4, Canada; Department of Electrical and Computer Engineering, Princeton University, Princeton, New Jersey 08544, United States

Alejandro W. Rodriguez — Department of Electrical and Computer Engineering, Princeton University, Princeton, New Jersey 08544, United States

Jacob J. Krich — Department of Physics, University of Ottawa, Ottawa, Ontario K1N 6N5, Canada; orcid.org/0000-0003-4514-0720

Karin Hinzer — SUNLAB, School of Electrical Engineering and Computer Science, University of Ottawa, Ottawa, Ontario K1N 6N5, Canada

Complete contact information is available at: <https://pubs.acs.org/10.1021/acs.nanolett.3c02049>

Notes

The authors declare no competing financial interest.

■ ACKNOWLEDGMENTS

This work was funded by the National Science and Engineering Research Council of Canada (No. NSERC CGS-D and No. NSERC 497981), the Ontario Graduate Scholarship (OGS), the New Frontiers in Research Fund (No. NFRFE-2019-00334), and by start-up funds from the Faculty of Engineering at the University of Ottawa.

■ REFERENCES

- Molesky, S.; Jacob, Z. Ideal near-field thermophotovoltaic cells. *Phys. Rev. B* **2015**, *91*, 205435.

- (2) Ilic, O.; Jablan, M.; Joannopoulos, J. D.; Celanovic, I.; Soljačić, M. Overcoming the black body limit in plasmonic and graphene near-field thermophotovoltaic systems. *Opt. Express* **2012**, *20*, A366–A384.
- (3) Ben-Abdallah, P.; Biehs, S.-A. Near-Field Thermal Transistor. *Phys. Rev. Lett.* **2014**, *112*, No. 044301.
- (4) Jin, W.; Molesky, S.; Lin, Z.; Rodriguez, A. W. Material scaling and frequency-selective enhancement of near-field radiative heat transfer for lossy metals in two dimensions via inverse design. *Phys. Rev. B* **2019**, *99*, No. 041403.
- (5) Zhu, L.; Otey, C. R.; Fan, S. Ultrahigh-contrast and large-bandwidth thermal rectification in near-field electromagnetic thermal transfer between nanoparticles. *Phys. Rev. B* **2013**, *88*, 184301.
- (6) Biehs, S.-A.; Rosa, F. S. S.; Ben-Abdallah, P. Modulation of near-field heat transfer between two gratings. *Appl. Phys. Lett.* **2011**, *98*, 243102.
- (7) Ben-Abdallah, P.; Belarouci, A.; Frechette, L.; Biehs, S.-A. Heat flux splitter for near-field thermal radiation. *Appl. Phys. Lett.* **2015**, *107*, No. 053109.
- (8) Laroche, M.; Carminati, R.; Greffet, J.-J. Near-field thermophotovoltaic energy conversion. *J. Appl. Phys.* **2006**, *100*, No. 063704.
- (9) Milovich, D.; Villa, J.; Antolin, E.; Datas, A.; Marti, A.; Vaillon, R.; Francoeur, M. Design of an indium arsenide cell for near-field thermophotovoltaic devices. *Journal of Photonics for Energy* **2020**, *10*, 1–18.
- (10) Fiorino, A.; Zhu, L.; Thompson, D.; Mittapally, R.; Reddy, P.; Meyhofer, E. Nanogap near-field thermophotovoltaics. *Nat. Nanotechnol.* **2018**, *13*, 806–811.
- (11) DiMatteo, R. S.; Greiff, P.; Finberg, S. L.; Young-Waithe, K. A.; Choy, H. K. H.; Masaki, M. M.; Fonstad, C. G. Micron-gap ThermoPhotoVoltaics (MTPV). *AIP Conf. Proc.* **2003**, *653*, 232–240.
- (12) Bhatt, G. R.; Zhao, B.; Roberts, S.; Datta, I.; Mohanty, A.; Lin, T.; Hartmann, J.-M.; St-Gelais, R.; Fan, S.; Lipson, M. Integrated near-field thermo-photovoltaics for heat recycling. *Nat. Commun.* **2020**, *11*, 2545.
- (13) Guha, B.; Otey, C.; Poitras, C. B.; Fan, S.; Lipson, M. Near-Field Radiative Cooling of Nanostructures. *Nano Lett.* **2012**, *12*, 4546–4550.
- (14) Howell, J. R.; Mengüç, M. P.; Daun, K.; Siegel, R. *Thermal Radiation Heat Transfer*, 7th ed.; CRC Press, 2020; pp 741–777.
- (15) Cravalho, E. G.; Tien, C. L.; Caren, R. P. Effect of Small Spacings on Radiative Transfer Between Two Dielectrics. *Journal of Heat Transfer* **1967**, *89*, 351–358.
- (16) Polder, D.; Van Hove, M. Theory of Radiative Heat Transfer between Closely Spaced Bodies. *Phys. Rev. B* **1971**, *4*, 3303–3314.
- (17) Pendry, J. B. Radiative exchange of heat between nanostructures. *J. Phys.: Condens. Matter* **1999**, *11*, 6621–6633.
- (18) Carminati, R.; Greffet, J.-J. Near-Field Effects in Spatial Coherence of Thermal Sources. *Phys. Rev. Lett.* **1999**, *82*, 1660–1663.
- (19) Volokitin, A. I.; Persson, B. N. J. Radiative heat transfer between nanostructures. *Phys. Rev. B* **2001**, *63*, 205404.
- (20) Babuty, A.; Joulain, K.; Chapuis, P.-O.; Greffet, J.-J.; De Wilde, Y. Blackbody Spectrum Revisited in the Near Field. *Phys. Rev. Lett.* **2013**, *110*, 146103.
- (21) Müller-Hirsch, W.; Kraft, A.; Hirsch, M. T.; Parisi, J.; Kittel, A. Heat transfer in ultrahigh vacuum scanning thermal microscopy. *Journal of Vacuum Science & Technology A* **1999**, *17*, 1205–1210.
- (22) Xu, J.; Läger, K.; Möller, R.; Dransfeld, K.; Wilson, I. H. Heat transfer between two metallic surfaces at small distances. *J. Appl. Phys.* **1994**, *76*, 7209–7216.
- (23) Kim, K.; Song, B.; Fernández-Hurtado, V.; Lee, W.; Jeong, W.; Cui, L.; Thompson, D.; Feist, J.; Reid, M. T. H.; García-Vidal, F. J.; et al. Radiative heat transfer in the extreme near field. *Nature* **2015**, *528*, 387–391.
- (24) Kloppstech, K.; Köne, N.; Biehs, S.-A.; Rodriguez, A. W.; Worbes, L.; Hellmann, D.; Kittel, A. Giant heat transfer in the crossover regime between conduction and radiation. *Nat. Commun.* **2017**, *8*, 14475.
- (25) Lucchesi, C.; Cakiroglu, D.; Perez, J.-P.; Taliercio, T.; Tournié, E.; Chapuis, P.-O.; Vaillon, R. Near-Field Thermophotovoltaic Conversion with High Electrical Power Density and Cell Efficiency above 14%. *Nano Lett.* **2021**, *21*, 4524–4529.
- (26) Song, B.; Ganjeh, Y.; Sadat, S.; Thompson, D.; Fiorino, A.; Fernández-Hurtado, V.; Feist, J.; Garcia-Vidal, F. J.; Cuevas, J. C.; Reddy, P.; et al. Enhancement of near-field radiative heat transfer using polar dielectric thin films. *Nat. Nanotechnol.* **2015**, *10*, 253–258.
- (27) van Zwol, P. J.; Ranno, L.; Chevrier, J. Tuning Near Field Radiative Heat Flux through Surface Excitations with a Metal Insulator Transition. *Phys. Rev. Lett.* **2012**, *108*, 234301.
- (28) Shen, S.; Mavrokefalos, A.; Sambegoro, P.; Chen, G. Nanoscale thermal radiation between two gold surfaces. *Appl. Phys. Lett.* **2012**, *100*, 233114.
- (29) Rousseau, E.; Siria, A.; Jourdan, G.; Volz, S.; Comin, F.; Chevrier, J.; Greffet, J.-J. Radiative heat transfer at the nanoscale. *Nat. Photonics* **2009**, *3*, 514–517.
- (30) Menges, F.; Dittberner, M.; Novotny, L.; Passarello, D.; Parkin, S. S. P.; Spieser, M.; Riel, H.; Gotsmann, B. Thermal radiative near field transport between vanadium dioxide and silicon oxide across the metal insulator transition. *Appl. Phys. Lett.* **2016**, *108*, 171904.
- (31) Narayanaswamy, A.; Shen, S.; Chen, G. Near-field radiative heat transfer between a sphere and a substrate. *Phys. Rev. B* **2008**, *78*, 115303.
- (32) Shi, K.; Sun, Y.; Chen, Z.; He, N.; Bao, F.; Evans, J.; He, S. Colossal Enhancement of Near-Field Thermal Radiation Across Hundreds of Nanometers between Millimeter-Scale Plates through Surface Plasmon and Phonon Polaritons Coupling. *Nano Lett.* **2019**, *19*, 8082–8088.
- (33) Lim, M.; Song, J.; Lee, S. S.; Lee, B. J. Tailoring near-field thermal radiation between metallo-dielectric multilayers using coupled surface plasmon polaritons. *Nat. Commun.* **2018**, *9*, 4302.
- (34) St-Gelais, R.; Zhu, L.; Fan, S.; Lipson, M. Near-field radiative heat transfer between parallel structures in the deep subwavelength regime. *Nat. Nanotechnol.* **2016**, *11*, 515–519.
- (35) Salihoglu, H.; Nam, W.; Traverso, L.; Segovia, M.; Venuthurumilli, P. K.; Liu, W.; Wei, Y.; Li, W.; Xu, X. Near-Field Thermal Radiation between Two Plates with Sub-10 nm Vacuum Separation. *Nano Lett.* **2020**, *20*, 6091–6096.
- (36) Ottens, R. S.; Quetschke, V.; Wise, S.; Alemi, A. A.; Lundock, R.; Mueller, G.; Reitze, D. H.; Tanner, D. B.; Whiting, B. F. Near-Field Radiative Heat Transfer between Macroscopic Planar Surfaces. *Phys. Rev. Lett.* **2011**, *107*, No. 014301.
- (37) Kralik, T.; Hanzelka, P.; Zobac, M.; Musilova, V.; Fort, T.; Horak, M. Strong Near-Field Enhancement of Radiative Heat Transfer between Metallic Surfaces. *Phys. Rev. Lett.* **2012**, *109*, 224302.
- (38) Ijro, T.; Yamada, N. Near-field radiative heat transfer between two parallel SiO₂ plates with and without microcavities. *Appl. Phys. Lett.* **2015**, *106*, No. 023103.
- (39) Ghashami, M.; Geng, H.; Kim, T.; Iacopino, N.; Cho, S. K.; Park, K. Precision Measurement of Phonon-Polaritonic Near-Field Energy Transfer between Macroscale Planar Structures Under Large Thermal Gradients. *Phys. Rev. Lett.* **2018**, *120*, 175901.
- (40) Hargreaves, C. Anomalous radiative transfer between closely-spaced bodies. *Phys. Lett. A* **1969**, *30*, 491–492.
- (41) Sabbaghi, P.; Long, L.; Ying, X.; Lambert, L.; Taylor, S.; Messner, C.; Wang, L. Super-Planckian radiative heat transfer between macroscale metallic surfaces due to near-field and thin-film effects. *J. Appl. Phys.* **2020**, *128*, No. 025305.
- (42) Tang, L.; DeSutter, J.; Francoeur, M. Near-Field Radiative Heat Transfer between Dissimilar Materials Mediated by Coupled Surface Phonon- and Plasmon-Polaritons. *ACS Photonics* **2020**, *7*, 1304–1311.
- (43) DiMatteo, R. S.; Greiff, P.; Finberg, S. L.; Young-Waithe, K. A.; Choy, H. K. H.; Masaki, M. M.; Fonstad, C. G. Enhanced photogeneration of carriers in a semiconductor via coupling across a nonisothermal nanoscale vacuum gap. *Appl. Phys. Lett.* **2001**, *79*, 1894–1896.

- (44) Hu, L.; Narayanaswamy, A.; Chen, X.; Chen, G. Near-field thermal radiation between two closely spaced glass plates exceeding Planck's blackbody radiation law. *Appl. Phys. Lett.* **2008**, *92*, 133106.
- (45) Ito, K.; Miura, A.; Iizuka, H.; Toshiyoshi, H. Parallel-plate submicron gap formed by micromachined low-density pillars for near-field radiative heat transfer. *Appl. Phys. Lett.* **2015**, *106*, No. 083504.
- (46) Lang, S.; Sharma, G.; Molesky, S.; Kränzien, P. U.; Jalas, T.; Jacob, Z.; Petrov, A. Y.; Eich, M. Dynamic measurement of near-field radiative heat transfer. *Sci. Rep.* **2017**, *7*, 13916.
- (47) Feng, C.; Tang, Z.; Yu, J.; Sun, C. A MEMS Device Capable of Measuring Near-Field Thermal Radiation between Membranes. *Sensors* **2013**, *13*, 1998–2010.
- (48) Nika, D. L.; Balandin, A. A. Two-dimensional phonon transport in graphene. *J. Phys.: Condens. Matter* **2012**, *24*, 233203.
- (49) Biehs, S.-A. Thermal heat radiation, near-field energy density and near-field radiative heat transfer of coated materials. *European Physical Journal B* **2007**, *58*, 423–431.
- (50) Shi, K.; Bao, F.; He, S. Enhanced Near-Field Thermal Radiation Based on Multilayer Graphene-hBN Heterostructures. *ACS Photonics* **2017**, *4*, 971–978.
- (51) Salihoglu, H.; Xu, X. Near-field radiative heat transfer enhancement using natural hyperbolic material. *Journal of Quantitative Spectroscopy and Radiative Transfer* **2019**, *222–223*, 115–121.
- (52) Moncada-Villa, E.; Fernández-Hurtado, V.; García-Vidal, F. J.; García-Martín, A.; Cuevas, J. C. Magnetic field control of near-field radiative heat transfer and the realization of highly tunable hyperbolic thermal emitters. *Phys. Rev. B* **2015**, *92*, 125418.
- (53) Basu, S.; Yang, Y.; Wang, L. Near-field radiative heat transfer between metamaterials coated with silicon carbide thin films. *Appl. Phys. Lett.* **2015**, *106*, No. 033106.
- (54) Giroux, M.; Zhang, C.; Snell, N.; Mu, G.; Stephan, M.; St-Gelais, R. High resolution measurement of near-field radiative heat transfer enabled by nanomechanical resonators. *Appl. Phys. Lett.* **2021**, *119*, 173104.
- (55) Ted Pella, Inc., PELCO® Silicon Nitride Support Films for TEM. 2007; https://www.tedpella.com/grids_html/silicon-nitride.aspx#_21597_10, Accessed on 2022-12-21.
- (56) Norcada, Silicon Nitride Membrane Windows for TEM Analysis. 2013; <https://www.norcada.com/products/nitride-windows-tem/>, Accessed on 2023-04-05.
- (57) Joulain, K.; Mulet, J.-P.; Marquier, F.; Carminati, R.; Greffet, J.-J. Surface electromagnetic waves thermally excited: Radiative heat transfer, coherence properties and Casimir forces revisited in the near field. *Surf. Sci. Rep.* **2005**, *57*, 59–112.
- (58) Antezza, M.; Pitaevskii, L. P.; Stringari, S.; Svetovoy, V. B. Casimir-Lifshitz force out of thermal equilibrium. *Phys. Rev. A* **2008**, *77*, No. 022901.
- (59) Anetsberger, G.; Arcizet, O.; Unterreithmeier, Q. P.; Rivière, R.; Schliesser, A.; Weig, E. M.; Kotthaus, J. P.; Kippenberg, T. J. Near-field cavity optomechanics with nanomechanical oscillators. *Nat. Phys.* **2009**, *5*, 909–914.
- (60) Garcia-Sanchez, D.; Fong, K. Y.; Bhaskaran, H.; Lamoreaux, S.; Tang, H. X. Casimir Force and In Situ Surface Potential Measurements on Nanomembranes. *Phys. Rev. Lett.* **2012**, *109*, No. 027202.
- (61) Lucchesi, C.; Vaillon, R.; Chapuis, P.-O. Radiative heat transfer at the nanoscale: experimental trends and challenges. *Nanoscale Horizons* **2021**, *6*, 201–208.
- (62) Thompson, D.; Zhu, L.; Mittapally, R.; Sadat, S.; Xing, Z.; McArdle, P.; Qazilbash, M. M.; Reddy, P.; Meyhofer, E. Hundred-fold enhancement in far-field radiative heat transfer over the blackbody limit. *Nature* **2018**, *561*, 216–221.
- (63) Song, B.; Thompson, D.; Fiorino, A.; Ganjeh, Y.; Reddy, P.; Meyhofer, E. Radiative heat conductances between dielectric and metallic parallel plates with nanoscale gaps. *Nat. Nanotechnol.* **2016**, *11*, 509–514.
- (64) Mu, G.; Snell, N.; Zhang, C.; Xie, X.; Tahvildari, R.; Weck, A.; Godin, M.; St-Gelais, R. Remote Actuation of Silicon Nitride Nanomechanical Resonators Using On-Chip Substrate Capacitors. *Journal of Microelectromechanical Systems* **2023**, *32*, 29–36.
- (65) Rugar, D.; Mamin, H. J.; Guethner, P. Improved fiber-optic interferometer for atomic force microscopy. *Appl. Phys. Lett.* **1989**, *55*, 2588–2590.
- (66) Zhang, C.; Giroux, M.; Nour, T. A.; St-Gelais, R. Thermal radiation sensing using high mechanical Q-factor silicon nitride membranes. *2019 IEEE SENSORS*. **2019**, 1–4.
- (67) Sadeghi, P.; Demir, A.; Villanueva, L. G.; Kähler, H.; Schmid, S. Frequency fluctuations in nanomechanical silicon nitride string resonators. *Phys. Rev. B* **2020**, *102*, 214106.
- (68) Zwickl, B. M.; Shanks, W. E.; Jayich, A. M.; Yang, C.; Bleszynski Jayich, A. C.; Thompson, J. D.; Harris, J. G. E. High quality mechanical and optical properties of commercial silicon nitride membranes. *Appl. Phys. Lett.* **2008**, *92*, 103125.
- (69) Zhang, C.; Giroux, M.; Nour, T. A.; St-Gelais, R. Radiative Heat Transfer in Freestanding Silicon Nitride Membranes. *Phys. Rev. Applied* **2020**, *14*, No. 024072.
- (70) St-Gelais, R.; Bhatt, G. R.; Zhu, L.; Fan, S.; Lipson, M. Hot Carrier-Based Near-Field Thermophotovoltaic Energy Conversion. *ACS Nano* **2017**, *11*, 3001–3009.
- (71) Francoeur, M.; Mengüç, M. P.; Vaillon, R. Spectral tuning of near-field radiative heat flux between two thin silicon carbide films. *J. Phys. D: Appl. Phys.* **2010**, *43*, No. 075501.
- (72) Schmid, S.; Villanueva, L. G.; Roukes, M. L. Fundamentals of nanomechanical resonators. *Springer* **2016**, *49*, 20–29.
- (73) Bergman, T. L.; Incropera, F. P.; DeWitt, D. P.; Lavine, A. S. *Fundamentals of heat and mass transfer*; John Wiley & Sons, 2011; pp 767–933.
- (74) Derjaguin, B. V.; Abrikosova, I. I.; Lifshitz, E. M. Direct measurement of molecular attraction between solids separated by a narrow gap. *Q. Rev. Chem. Soc.* **1956**, *10*, 295–329.
- (75) Kitamura, R.; Pilon, L.; Jonasz, M. Optical constants of silica glass from extreme ultraviolet to far infrared at near room temperature. *Appl. Opt.* **2007**, *46*, 8118–8133.
- (76) Cataldo, G.; Beall, J. A.; Cho, H.-M.; McAndrew, B.; Niemack, M. D.; Wollack, E. J. Infrared dielectric properties of low-stress silicon nitride. *Opt. Lett.* **2012**, *37*, 4200–4202.
- (77) Senturia, S. D. *Microsystem design*; Kluwer Academic Publishers: Boston, MA, 2001; p 196.
- (78) Toivola, Y.; Thurn, J.; Cook, R. F.; Cibuzar, G.; Roberts, K. Influence of deposition conditions on mechanical properties of low-pressure chemical vapor deposited low-stress silicon nitride films. *J. Appl. Phys.* **2003**, *94*, 6915–6922.
- (79) Carlotti, G.; Colpani, P.; Piccolo, D.; Santucci, S.; Senez, V.; Socino, G.; Verdini, L. Measurement of the elastic and viscoelastic properties of dielectric films used in microelectronics. *Thin Solid Films* **2002**, *414*, 99–104.
- (80) Zhu, S.-E.; Krishna Ghatkesar, M.; Zhang, C.; Janssen, G. C. A. M. Graphene based piezoresistive pressure sensor. *Appl. Phys. Lett.* **2013**, *102*, 161904.
- (81) Petersen, K. Dynamic micromechanics on silicon: Techniques and devices. *IEEE Trans. Electron Devices* **1978**, *25*, 1241–1250.
- (82) Zhang, C.; St-Gelais, R. Demonstration of frequency stability limited by thermal fluctuation noise in silicon nitride nanomechanical resonators. *Appl. Phys. Lett.* **2023**, *122*, 193501.
- (83) Snell, N.; Zhang, C.; Mu, G.; Bouchard, A.; St-Gelais, R. Heat Transport in Silicon Nitride Drum Resonators and its Influence on Thermal Fluctuation-Induced Frequency Noise. *Phys. Rev. Appl.* **2022**, *17*, No. 044019.
- (84) DeSutter, J.; Tang, L.; Francoeur, M. A near-field radiative heat transfer device. *Nat. Nanotechnol.* **2019**, *14*, 751–755.
- (85) Metzger, C.; Ludwig, M.; Neuenhahn, C.; Ortlieb, A.; Favero, I.; Karrai, K.; Marquardt, F. Self-Induced Oscillations in an Optomechanical System Driven by Bolometric Backaction. *Phys. Rev. Lett.* **2008**, *101*, 133903.